Article

Quantum Dynamics Simulations of Interfacial Electron Transfer in Sensitized TiO Semiconductors

Luis G. C. Rego, and Victor S. Batista

J. Am. Chem. Soc., **2003**, 125 (26), 7989-7997• DOI: 10.1021/ja0346330 • Publication Date (Web): 10 June 2003

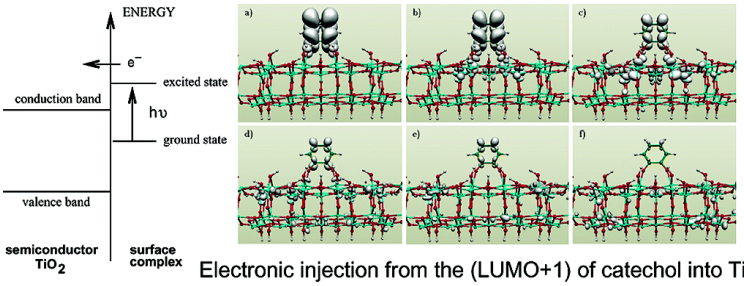

Electronic injection from the (LUMO+1) of catechol into TiO_2

More About This Article

Additional resources and features associated with this article are available within the HTML version:

- Supporting Information
- Links to the 27 articles that cite this article, as of the time of this article download
- Access to high resolution figures
- Links to articles and content related to this article
- Copyright permission to reproduce figures and/or text from this article

View the Full Text HTML

J|A|C|S
ARTICLES
Published on Web 06/10/2003

Quantum Dynamics Simulations of Interfacial Electron Transfer in Sensitized TiO_2 Semiconductors

Luis G. C. Rego and Victor S. Batista*

Contribution from the Department of Chemistry, Yale University, P.O. Box 208107, New Haven, Connecticut 06520-8107

Received February 12, 2003; E-mail: lrego@fisica.ufpr.br; victor.batista@yale.edu

Abstract: Ab initio DFT molecular dynamics simulations are combined with quantum dynamics calculations of electronic relaxation to investigate the interfacial electron transfer in catechol/TiO_2-anatase nanostructures under vacuum conditions. It is found that the primary process in the interfacial electron-transfer dynamics involves an ultrafast ($\tau_1 \simeq 6$ fs) electron-injection event that localizes the charge in the Ti^{4+} surface ions next to the catechol adsorbate. The primary event is followed by charge delocalization (i.e., carrier diffusion) through the TiO_2-anatase crystal, an anisotropic diffusional process that can be up to an order of magnitude slower along the [−101] direction than carrier relaxation along the [010] and [101] directions in the anatase crystal. It is shown that both the mechanism of electron injection and the time scales for interfacial electron transfer are quite sensitive to the symmetry of the electronic state initially populated in the adsorbate molecule. The results are particularly relevant to the understanding of surface charge separation in efficient mechanisms of molecular-based photovoltaic devices.

I. Introduction

Interfacial electron transfer between sensitizer molecular adsorbates and semiconductor materials has been a subject of intense research in recent years.[1−5] This is a fundamental process in surface chemistry, relevant to a broad range of practical applications, including effective mechanisms of solar energy conversion,[6,7] photoelectrochemistry,[8] artificial photosynthesis[9] and imaging.[10] Despite its great technological significance, interfacial electron transfer remains poorly understood[1,2] compared to electron transfer in homogeneous solutions.[11−14] In particular, there is still considerable controversy about the time scale and nature of the primary electron-transfer process in dye-sensitized TiO_2 electrodes. In this paper, ab initio DFT molecular dynamics simulations are combined with quantum dynamics calculations of electronic relaxation to investigate the interfacial electron transfer in catechol/TiO_2-anatase nanostructures.

Surface sensitization involves the adsorption of an organic molecule to a semiconductor surface and the formation of a surface complex. Photoexcitation of the surface complex can lead to interfacial electron transfer when there is suitable energy match between the photoexcited electronic state in the surface complex and the electronic states in the conduction band of the semiconductor (see Figure 1). Injection times as short as a few femtoseconds have been reported for various systems,[15,16] revealing that nuclear motion cannot be the rate-determining factor in the underlying interfacial electron-transfer mechanisms. The description of such ultrafast spectroscopic measurements thus seems to be beyond the capabilities of the traditional electron-transfer theory, where the nuclear reorganization plays

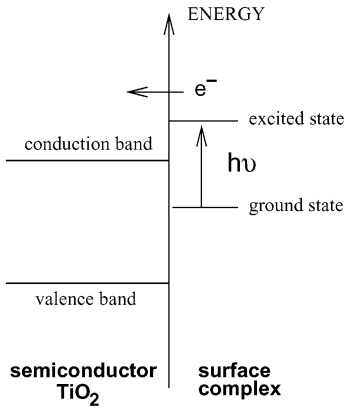

Figure 1. Energy diagram for dye sensitization of TiO_2. The diagram shows the energy levels of the surface complex, the photoexcitation process (see vertical arrow), and the electron injection in the conduction band of host material (horizontal arrow).

(1) Miller, R. J. D.; McLendon, G.; Nozik, A.; Willing, F.; Schimickler, W. In *Surface Electron-Transfer Processes*; VCH: New York, 1995.
(2) Nozik, A.; Memming, R. *J. Phys. Chem.* **1996**, *100*, 13061.
(3) Gratzël, A. H. M. *Chem. Rev.* **1995**, *95*, 49.
(4) Kamat, P.; Meisel, D. In *Semiconductor Nanocluster-Physical, Chemical and Catalytic Aspects*; Elsevier: Amsterdam, 1997.
(5) Bauer, C.; Boschloo, G.; Mukhtar, E.; Hagfeldt, A. *J. Phys. Chem. B* **2002**, *106*, 12693.
(6) O'Regan, B.; Grätzel, M. *Nature* **1991**, *353*, 737. O'Regan, B.; Grätzel, M. *Nature* **2001**, *414*, 338.
(7) Grätzel, A. H. M. *Acc. Chem. Res.* **2000**, *33*, 269.
(8) Fujishima, A.; Honda, K. *Nature* **1972**, *238*, 37.
(9) Kalayanasundaram, K.; Grätzel, M. *Coord. Chem. Rev.* **1998**, *77*, 347.
(10) Jacobson, K.; Jacobson, R. In *Imaging Systems*; John Wiley & Sons: New York, 1976.
(11) Newton, M.; *Chem. Rev.* **1991**, *91*, 767.
(12) Barbara, P.; Meyer, T.; Ratner, M. *J. Phys. Chem.* **1996**, *100*, 13148.
(13) Marcus, R.; Sutin, N. *Biochim. Biophys. Acta* **1985**, *811*, 265.
(14) Boroda, Y. G.; Calhoun, A.; Voth, G. A. *J. Chem. Phys.* **1997**, *107*, 8940.
(15) Schnadt, J.; et al. *Nature* **2002**, *418*, 620.
(16) Huber, R.; Moser, J. E.; Grätzel, M.; Wachtveitl, J. *J. Phys. Chem. B* **2002**, *106*, 6494.

a central role in determining the electron-transfer rates. It is, therefore, essential to combine experimental studies with realistic theoretical simulations to develop a comprehensive understanding of the underlying electron-transfer dynamics.

Quantum chemistry calculations of small organic molecules adsorbed to semiconductor surfaces have been reported, including studies of aromatic adsorbates on metal oxide substrates.[17] Particularly, there have been studies of formic acid[18] or bi-isonicotinic acid[19] anchored to the (110) surface of TiO_2-rutile and HCOOH[20] or bi-isonicotinic acid[21] anchored to the (101) surface of TiO_2-anatase. However, the complexity of the interface has limited the capabilities of quantum chemistry calculations to solve a number of fundamental aspects (e.g., it is still unclear how strongly intermediate excited-states in the molecular adsorbate couple to the conduction band of TiO_2 and what is the role of these states in the photoinduced electron-injection mechanism). The complexity of the problem has also limited quantum dynamics simulations to the implementation of approximate schemes. Smith and Nozik have investigated 1-dimensional and 3-dimensional model systems in an effort to understand the central aspects of interfacial electron transfer as well as the limitations of theoretical approaches such as the Landau−Zener approximation[22] and the Anderson Hamiltonian approach.[23] Marcus and co-workers have extended the theoretical formalism originally developed for homogeneous reactions. These authors have explored electron transfer in solid−liquid systems by using the Fermi Golden Rule in conjunction with the tight-binding method[24] or the free electron model[25] for the description of the electronic structure. Prezhdo and co-workers have recently implemented a surface hopping approach to the description of nonadiabatic dynamics in the isonicotinic acid/TiO_2-rutile complex.[26] In this paper we investigate the process of electron injection in catechol/TiO_2-anatase nanostructures at the detailed molecular level.

The photoinduced electron transfer in the catechol/anatase system has yet to be probed by ultrafast spectroscopic measurements. However, the charge-transfer effect has already been assigned to the 420−430 nm absorption band in UV/vis transmittance measurements for nanometer-sized particle suspensions as well as in UV/vis differential diffuse reflectance measurements for dried 30-nm powders of TiO_2-anatase with adsorbed catechol.[27,28] In addition, a semiempirical study[29] has assigned the absorption band at 420 nm to a *direct* charge-transfer excitation from the catechol π orbital to the Ti^{4+} (3d) levels at the bottom of the TiO_2 conduction band. Furthermore, the charge-transfer band of catechol adsorbed on 0.4 μm sized TiO_2 (anatase) colloidal particles in aqueous suspensions has been observed at 456 nm, in the second-harmonic spectrum of the system.[30] These measurements also estimated a catechol monolayer density of 1.25 μmol m^{-2} (i.e., 1 catechol molecule per $\simeq$132 Å^2) from a Langmuir fit of the equilibrium constant for the adsorption of catechol on TiO_2-anatase.

Catechol has raised significant interest as a model sensitizer not only because it significantly lowers the absorption threshold of TiO_2 from 370 to 420 nm but also because it constitutes sensitizers with high incident photon-to-current conversion efficiencies (e.g., photon-to-current conversion efficiencies of up to 50% have been measured on TiO_2-anatase surfaces sensitized by catechol para-substituted with Ru(II)-polypyridyl complexes[31]). These sensitizers thus show considerable promise in the development of photovoltaic cells. Contrary to a direct charge-transfer excitation, these efficient photoinjection mechanisms involve electronic excited states in the molecular adsorbate. The simulations of electron injection investigated in this work aim to gain a fundamental understanding of such excited-state electron-injection paths.

Realistic simulations of heterogeneous electron-transfer processes face the challenge of modeling quantum dynamics in large model systems, since finite size effects or even artificial periodic boundary conditions can produce inaccurate results (e.g., recurrent electron-transient populations). In addition, to account for the ultrafast electronic relaxation in the host material, a reliable description of the electronic couplings between the discrete molecular states in the anchored molecule and the dense manifold of highly delocalized electronic levels in the semiconductor is required. In the event that the time scales associated with the electronic relaxation are much faster than the nuclear motion, it is possible to implement a simplified procedure to investigate the excited-state electron transfer at the detailed molecular level, that is, assuming the decoupling of the electronic and nuclear dynamics.

To investigate interfacial electron transfer in sufficiently extended model systems, representative nuclear configurations are obtained according to ab initio DFT molecular dynamics simulations, and the time-dependent electronic wave function is propagated according to a model Hamiltonian gained from the semiempirical extended Hückel (EH) approach. The role that symmetry plays in the electron-injection mechanism is investigated by computing the time-dependent electron density after photoexcitation of the adsorbate chromophore to the catechol-LUMO and catechol-(LUMO+1) in TiO_2 nanostructures extended along different crystallographic directions.

The simulation results described in this paper show the first direct evidence of an anisotropic electron-injection mechanism and the origin of multiple time scales associated with the process of carrier relaxation. The interfacial electron-transfer involves an ultrafast ($\tau \simeq 6$ fs) primary electron-transfer event that localizes the charge on the Ti^{4+} surface ions next to the adsorbate molecule. This primary injection event is followed by an anisotropic delocalization process, which can be up to an order of magnitude slower along the [−101] direction than along the [010] or the [101] crystallographic directions in the anatase crystal. It is shown that both the primary electron-injection event and the anisotropic relaxation of the injected charge are quite sensitive to the symmetry of the initially populated electronic

(17) Persson, P.; Lunell, S.; Ojamae, L. *Chem. Phys. Lett.* **2001**, *364*, 469.
(18) Käckell, P.; Terakura, K. *Surf. Sci.* **2000**, *461*, 191.
(19) Persson, P.; Stashans, A.; Bergström, R.; Lunell, S. *Int. J. Quantum Chem.* **1998**, *70*, 1055.
(20) Vittadini, A.; Selloni, A.; Rotzinger, F. P.; Grätzel, M. *J. Phys. Chem. B* **2000**, *104*, 1300.
(21) Persson, P.;Lunell, Sten *Sol. Energy Mater. Sol. Cells* **2000**, *63*, 139.
(22) Smith, B. B.; Nozik, A. J. *J. Phys. Chem.* B **1999**, *103*, 9915.
(23) Smith, B. B.; Nozik, A. *J. Chem. Phys.* **1996**, *205*, 47.
(24) Gao, Y. Q.; Georgievskii, Y.; Marcus, R. A. *J. Chem. Phys.* **2000**, *112*, 3358.
(25) Gao, Y. Q.; Marcus, R. A. *J. Chem. Phys.* **2000**, *113*, 6351.
(26) Stier, W.; Prezhdo, O. V. *J. Phys. Chem B* **2002**, *106*, 8047.
(27) Moser, J.; Punchihewa, S.; Infelta, P. P.; Gratzel, M. *Langmuir* **1991**, *7*, 3012.
(28) Rodriguez, R.; Blesa, M. A.; Regazzoni, E. *J. Colloidal Interface. Sci.* **1996**, *177*, 122.
(29) Persson, P.; Bergström, R.; Lunell, S. *J. Phys. Chem. B* **2000**, *104*, 10348.
(30) Liu, Y.; Dadap, J. I.; Zimdars, D.; Eisenthal, K. B. *J. Phys. Chem. B* **1999**, *103*, 2480.
(31) Rice, C. R.; Ward, M. D.; Nazeeruddin, M. K.; Grätzel, M. *New J. Chem.* **2000**, *24*, 651.

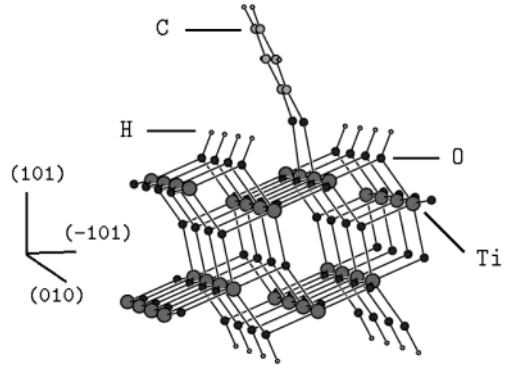

Figure 2. Unrelaxed configuration of the TiO_2-anatase model nanostructure sensitized by a catechol molecule anchored on the (101) surface of the crystal under vacuum conditions. Large gray spheres represent Ti^{4+} ions, black spheres are O^{2-} ions, medium light-gray spheres are C atoms, and small light spheres are H atoms.

state in the molecular adsorbate, since electron injection is primarily driven by the electronic couplings between the initially populated electronic state in the molecular adsorbate and the delocalized electronic states of similar energy in the semiconductor. Since the electronic couplings are expected to be only slightly perturbed by the interactions of the surface complex with solvating molecules, the relaxation processes reported in this paper are likely to be common not only to similar sensitized nanostructures under vacuum conditions but also to sensitized nanostructures in solutions.

The paper is organized as follows. Section II describes the catechol/TiO_2-anatase model system in terms of the crystallographic structure, the phonon spectral density, and the electronic density of states. Section II.C describes the simulations of electron injection and the calculation of transient populations. Section III.A presents the results of simulations of electron injection. Section III.B presents a discussion of the results. Section IV summarizes and concludes.

II. Model System

The model system is initially defined according to the unrelaxed anatase nanostructure depicted in Figure 2.

The nanostructure is composed of 32 [TiO_2] units, with bond lengths and angles initially defined according to ref 32. The catechol molecule is adsorbed to the (101) surface of the TiO_2-anatase crystal and forms a surface complex with two neighboring pentacoordinated Ti^{4+} ions. Dangling bonds in both the upper and lower surfaces of the slab are saturated with hydrogen atoms to avoid unphysical low coordination numbers and to make negligible the interaction between distinct slab surfaces in the infinitely periodic model system. The dimensions of the nanostructure are 10.22 Å × 15.13 Å × 30.95 Å in the [−101], [010], and [101] directions, respectively. The cell dimensions correspond to a monolayer density of 1 catechol molecule per 155 Å^2 (i.e., ∼1 μmol m^{-2}). A vacuum spacer is employed between slabs.

Figure 3 shows the relaxed nanostructure unit after fully optimizing the energy of the system with respect to the geometry of the anchored catechol molecule and the six topmost layers in the semiconductor surface, including the capping hydrogen atoms in the upper layer. Figure 3 shows that, far from the attachment site, the geometry of the anatase crystal is in agreement with previous theoretical calculations of TiO_2-anatase.[33] The largest conformational changes involve geometry rearrangements associated with the Ti^{4+} and O^{2-} ions next to the molecular adsorbate (see Figure 4) as well as the alignment of the catechol adsorbate along the [100] direction due to its electronic repulsion with the nearby row of dicoordinated O^{2-} ions. This electrostatic repulsion is also responsible for displacing the 2-fold coordinated O^{2-} ions and for stretching their bonds with the hexacoordinated Ti^{4+} ions next to the molecular adsorbate.

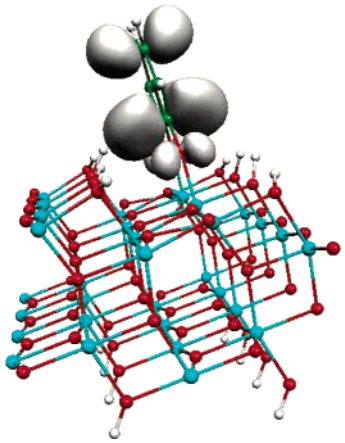

Figure 3. Nanostructure of TiO_2-anatase sensitized by catechol after geometry relaxation under vacuum conditions and electronic density in the highest occupied molecular orbital. The blue, red, green, and white spheres represent Ti^{4+} ions, O^{2-} ions, C atoms, and H atoms, respectively.

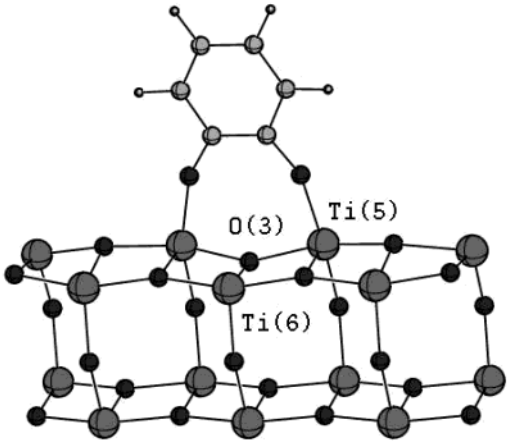

Figure 4. Local geometry of the relaxed nanostructure next to the catechol adsorbate. Ti(5) indicates one of the pentacoordinated Ti^{4+} ions directly anchoring the catechol adsorbate. Ti(6) labels the hexacoordinated Ti^{4+} ion next to the adsorbate.

In addition, both of the Ti^{4+} ions anchoring the catechol molecule are displaced outward relative to the (100) plane of the crystal. The 3-fold coordinated O^{2-}, connected to both of these Ti^{4+} ions, is displaced inward relative to the (100) plane of the crystal. Such rearrangement locates the displaced O^{2-} ion at a more equidistant position (i.e., at ∼1.924 Å) relative to its three nearest Ti^{4+} ions. This O^{2-} ion reaches such a position by moving out of the plane defined by the three nearest Ti^{4+} ions. The relaxed geometry is, therefore, significantly different from the initial configuration where the corresponding bond

(32) Burdett, J. K.; Hughbanks, T.; Miller, G. J.; Richardson, J. W.; Jr., Smith, J. V. *J. Am. Chem. Soc.* **1987**, *109*, 3639.
(33) Vittadini, A.; Selloni, A.; Rotzinger, F. P.; Grätzel, M. *Phys. Rev. Lett.* **1998**, *81*, 2954.

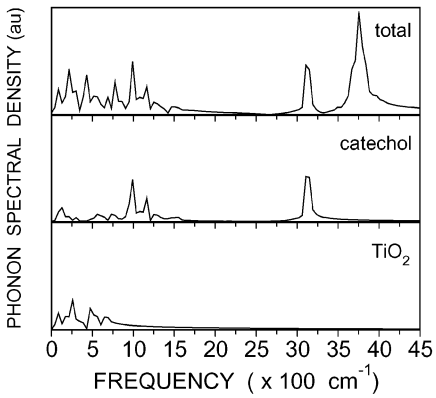

Figure 5. Upper panel: total phonon spectral density of the catechol/TiO_2-anatase model system described in section II. Middle panel: contributions to the phonon spectral density due to nuclear motion in the catechol molecule. Lower panel: contributions to the phonon spectral density due to ionic nuclear motion in the TiO_2-anatase semiconductor, excluding the O−H stretching model peak produced by the H capping atoms.

distances are 1.979 Å (hexacoord Ti−O) and 1.932 Å (for both pentacoord Ti−O).[32] Section III shows that the two Ti^{4+} ions directly anchoring the molecular adsorbate as well as the hexacoordinated Ti^{4+} ion next to the adsorbate (refer to Figure 4) play crucial roles in the excited-state interfacial electron-transfer mechanisms.

The geometry of the nanostructure has been optimized with the Vienna ab initio simulation package (VASP/VAMP),[34,35] implementing the density functional theory (DFT) to treat the Hartree and exchange-correlation electronic interactions. The Perdew−Wang[36] generalized gradient approximation was implemented for the exchange-correlation functional, in conjunction with ultrasoft Vanderbilt pseudopotentials[37] to describe the ionic interactions. The Kohn−Sham (KS) Hamiltonian was projected onto a plane-wave basis set and high-efficiency iterative methods were implemented to obtain the KS eigenstates and eigenvalues. Self-consistency was accelerated by means of efficient charge density mixing schemes. Calculations were performed in an SP2 supercomputer cluster to take full advantage of the parallelized version of the code.

A. Phonon Spectral Density. The upper panel of Figure 5 shows the total phonon spectral density of the catechol/TiO_2-anatase model system described in section II. The phonon spectral density has been computed as the Fourier transform of the velocity autocorrelation function obtained from ab initio DFT molecular dynamics simulations at 100 K and constant volume. The middle and lower panels of Figure 5 show the contributions to the total spectral density due to nuclear motion associated with the catechol molecule and the TiO_2-anatase semiconductor, respectively.

Note that the vibrational frequencies for both the catechol molecule and the TiO_2-anatase semiconductor are in good agreement with the experimental normal-mode frequencies reported in refs 38−40, respectively.

The more prominent peaks in the total spectral density, at 3700 and 3100 cm^{-1}, correspond to the O−H stretching motion of H capping atoms on the TiO_2-anatase surface and the C−H stretching motion in the catechol molecule, respectively. The high-frequency C−H mode involves the σ bonding between the hydrogen s orbital and the sp^2 hybridized orbital of the C atom. Therefore, this mode is essentially uncoupled from the electron-injection mechanism where the π-molecular orbitals of the molecular adsorbate and the d orbitals of the Ti^{4+} ions play a crucial role. The normal modes of TiO_2-anatase are in the 262−876 cm^{-1} range, in agreement with experimental measurements.[40] Therefore, the shortest period for vibrational ionic motion is approximately 40 fs. These vibrational periods are expected to be only marginally affected by photoexcitation of the adsorbate molecule, or the injection of an electron into the conduction band. Note that even the vibrational frequencies of the catechol molecule are only slightly affected by photoexcitation of the molecule to the S1 electronic state.[39] Section III shows that this characteristic time of 40 fs is an order of magnitude larger than the ultrafast time scale associated with the primary electron-injection event, or carrier relaxation along the [010] or [101] crystallographic directions in the anatase crystal.

B. Electronic Structure. The electronic structure of the model system introduced in section II is described according to a model Hamiltonian gained from the semiempirical EH approach. The EH method has been extensively implemented in calculations of the electronic structure of periodic systems. It has been shown that the method requires a relatively small number of transferable parameters and is capable of providing accurate results for the energy bands of elemental materials (including transition metals) as well as compound bulk materials in various phases.[41] The EH method is applicable to large extended systems and, contrary to plane-wave basis set approaches, provides valuable insight on the role of chemical bonding.[42] The method is, therefore, most suitable to develop a clear chemical picture of the interfacial electron-transfer mechanism at the semiquantitative level. Section III shows that the EH approach provides fundamental insight on the role that symmetry plays in the hybridization between excited-state molecular orbitals of the catechol adsorbate and the d orbitals of the nearby Ti^{4+} ions in the TiO_2 crystal. Such hybridization is responsible for the electronic couplings that drive the interfacial electron-transfer dynamics.

The EH Hamiltonian is computed in the basis of Slater-type orbitals for the radial part of the atomic orbital (AO) wave functions.[43,44] The basis set includes the 3d, 4s, and 4p atomic orbitals of Ti^{4+} ions, the 2s and 2p atomic orbitals of O^{2-} ions, the 2s and 2p atomic orbitals of C atoms, and the 1s atomic orbitals of H atoms. This amounts to a set of 596 basis functions for the representation of the Hamiltonian matrix associated with the nanostructure shown in Figure 3. The diagonalization of this Hamiltonian matrix yields the density of states shown in Figure 6.

(34) http://cms.mpi.univie.ac.at/vasp/.
(35) Kresse, G. *Phys. Rev. B* **1996**, *54*, 11169; Kresse, G.; Furthmüller, J. *Comput. Mater. Sci.* **1996**, *6*, 15.
(36) Perdew, J. In *Electronic Structure of Solids*; Ziesche, P., Eschrig, H., Eds.; Verlag: Berlin, 1991.
(37) Vanderbilt, D. *Phys. Rev. B* **1990**, *41*, 7892.
(38) Wilson, H. W. *Spectrochim. Acta Part A* **1974**, *30*, 2141.
(39) Gerhards, M.; Perl, W.; Schumm, S.; Henrichs, U.; Jacoby, C.; Kleinermanns, K. *J. Chem. Phys.* **1996**, *104*, 9362.
(40) Gonzalez, R. J.; Zallen, R. *Phys. Rev. B* **1997**, *55*, 7014.
(41) Cerda, J.; Soria, F. *Phys. Rev. B* **2000**, *61*, 7965.
(42) Hoffmann, R. *Rev. Mod. Phys.* **1988**, *60*, 601.
(43) McGlynn, S. P.; Vanquickenborne, L. G.; Kinoshita, M.; Carroll, D. G. *Introduction to Applied Quantum Chemistry*; Holt, Rinehart and Winston INC.: New York, 1972.
(44) For a numerical implementation of the method: Landrum, G. A.; Glassy, W. V. *The YAeHMOP project*, http://yaehmop.sourceforge.net.

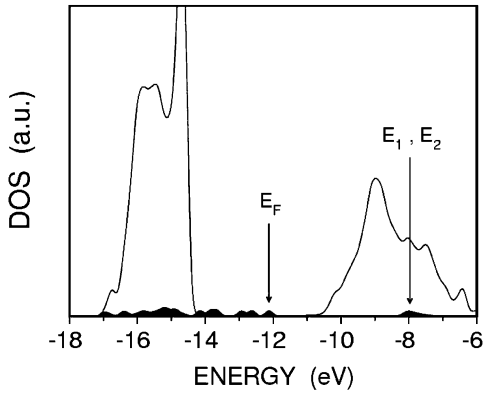

Figure 6. Density of states for the relaxed nanostructure shown in Figure 3. The filled solid curve at the bottom of the graph represents the projected density of states on the catechol basis functions. The Fermi energy E_F indicates the HOMO of the system. States E_1 and E_2 represent the excited electronic states with a predominant contribution of the catechol LUMO and (LUMO+1), respectively. The distribution of eigenvalues has been convoluted with a Gaussian function (FWHM = 0.5 eV) to facilitate its visualization.

Figure 6 shows that the EH Hamiltonian predicts a 3.7 eV band gap for the 1.2 nm model system, introduced in section II. This result is in good agreement with the 3.7 eV excitation energy computed by Bredow and Jug,[45] according to the semiempirical SINDO1 method as implemented for the TiO_2-anatase nanoparticles $Ti_{21}O_{38}H_4(OH)_{12}$ and $Ti_{97}O_{186}(OH)_{16}$. The computed band gap is also consistent with the experimental values of 3.2 eV for the band gap in the bulk TiO_2-anatase and 3.4 eV in 2.4 nm particles[46] since the band gap for smaller nanoparticles is expected to be somewhat larger than the band gap in larger systems.

The filled solid curve at the bottom of the graph in Figure 6 represents the projected density of states on the catechol basis functions. This curve shows that the catechol molecule introduces electronic states in the semiconductor band gap (i.e., sensitizes the semiconductor). Furthermore, Figure 6 shows that the catechol molecule introduces excited electronic states (e.g., excited electronic states E_1 and E_2 with predominant contributions from the catechol-LUMO and catechol-(LUMO+1), respectively) that overlap in energy with electronic states in the conduction band of the TiO_2-anatase semiconductor. The electronic states at the bottom of the conduction band have a predominant projection onto the $3d_{xz}$, $3d_{yz}$, and $3d_{xy}$ orbitals of Ti^{4+} (see also refs 48 and 32). Section III shows that these 3d orbitals of Ti^{4+} ions are responsible for delocalizing the charge injected from the E_1 or E_2 electronic states.

C. Simulations of Electron Injection. The quantity of interest is the survival probability $\rho_{MOL}(t)$ defined as the probability that at time t, after excitation of the system, the electron is still in the adsorbate molecule. Therefore, $\rho_{MOL}(t)$ can be computed by projecting the time-evolved electronic wave function onto the atomic orbitals of the molecular adsorbate.

The time-evolved wave function $|\Phi(t)\rangle$ is written as a linear combination of atomic orbitals

$$|\Phi(t)\rangle = \sum_{i,\alpha} B_{i,\alpha}(t)|i,\alpha\rangle \qquad (1)$$

where $|i,\alpha\rangle$ represents the atomic orbital α of atom i. The expansion coefficients $B_{i,\alpha}(t)$, introduced in eq 1, are computed according to

$$B_{i,\alpha}(t) = \sum_q Q_{i,\alpha}{}^q C_q e^{-(i/\hbar)E_q t} \qquad (2)$$

after solving the generalized eigenvalue problem

$$HQ^q = E_q S Q^q \qquad (3)$$

where H is the EH matrix and S is the overlap matrix in the atomic orbital basis. The coefficients C_q, introduced in eq 2, are defined by the expansion of the initial state in the orthonormal basis set of eigenvectors $|q\rangle$,

$$|\Phi(0)\rangle = \sum_q C_q|q\rangle \qquad (4)$$

The coefficients $Q^q{}_{i,\alpha}$, introduced in eq 2, are defined according to the expansion of the eigenvectors $|q\rangle$ as a linear combination of atomic orbitals,

$$|q\rangle = \sum_{i,\alpha} Q_{i,\alpha}{}^q|i,\alpha\rangle \qquad (5)$$

The projection of the time-evolved electronic wave function onto the atomic orbitals of the molecular adsorbate is, therefore, obtained according to the equation

$$\rho_{MOL}(t) = |\sum_{i,\alpha}^{MOL} \sum_{j,\beta} B_{i,\alpha}{}^*(t)B_{j,\beta}(t)S^{i,j}_{\alpha,\beta}| \qquad (6)$$

Here $S^{i,j}_{\alpha\beta} = \langle i,\alpha|\, j,\beta\rangle$, where the indices α and β label specific orbitals in atoms i and j, respectively. Note that the sum over j includes all of the atoms in the nanostructure, whereas the sum over i includes only atoms in the initially excited molecular adsorbate.

To avoid recurrences in electron-transient populations, due to the finite size of the nanostructure, it is necessary to add an absorbing potential (i.e., an imaginary term to the diagonal elements of H that correspond to Ti^{4+} ions located at the nanostructure boundary surfaces). Note that by adding this absorbing potential, H becomes non-Hermitian and the basis set $|q\rangle$ becomes nonorthogonal. To compute $\rho_{MOL}(t)$, in accord with eq 6, it is therefore necessary to work with the left and right eigenvectors of H, $|q^L\rangle$ and $|q^R\rangle$, respectively.

III. Results and Discussion

Section III presents the comparison of electron injection from the catechol-LUMO and the catechol-(LUMO+1) into the TiO_2-anatase semiconductor. As mentioned in section II.B, these states are important components of the excited-electronic structure responsible for electron injection in larger dyes (e.g., catechol para-substituted with Ru(II)-polypyridyl complexes) since they match in energy with the lower manifold of electronic states in the conduction band (see Figure 6).

A. Electron-Injection Mechanism. The nanostructure introduced in section II is expected to manifest finite size effects in the description of electron transfer as soon as the injected charge reaches the edges of the cluster. It is, therefore, important

(45) Bredow, T.; Jug, K. *J. Phys. Chem.* **1998**, *92*, 5196.

(46) Korman, C.; Bahnemann, D. W.; Hoffman, M. R. *J. Phys. Chem.* **1998**, *92*, 5196.

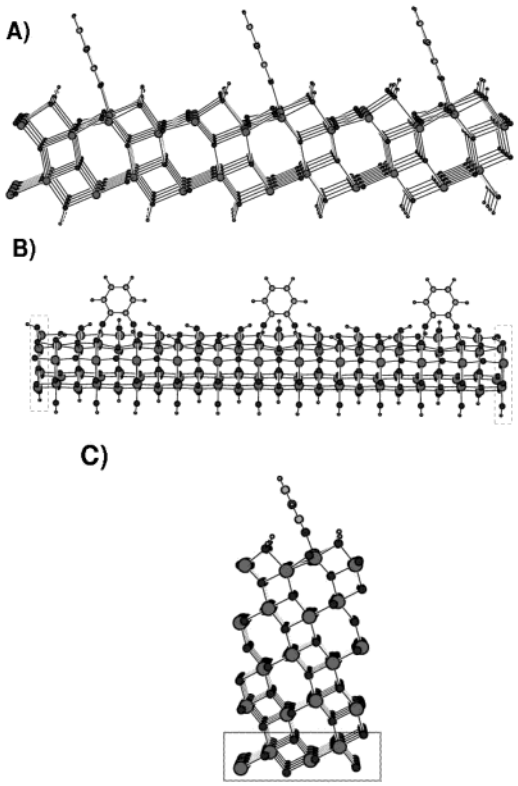

Figure 7. Panels A, B, and C show nanostructures extended along the [−101], [010], and [101] directions in the anatase crystal. The box in panels B and C indicates the layer of Ti^{4+} ions with an absorbing potential. In addition, periodic boundary conditions are applied to all structures along the nonextended direction, that is, the [010] for panel A and along the [−101] for panels B and C.

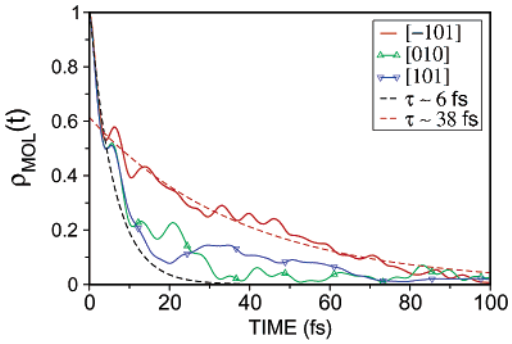

Figure 8. Time-dependent survival probability in sensitized nanostructures extended along the [−101], [010], and [101] crystallographic direction in the TiO_2 anatase crystal. The electronic excitation is initialized by populating the catechol-LUMO. The dashed lines are exponential fitting curves to the two elementary steps for electron transfer in the nanostructure extended along the [−101] direction.

to analyze the convergence properties of the simulation results with respect to the size of the system. This is accomplished by checking convergence in the electron injection times in nanostructures extended along the [−101], [010], and [101] crystallographic directions with 1, 3, and 5 nanostructure units. Figure 7 shows extended structures generated by replicating nanostructure units along the three crystallographic directions.

1. Electron Injection from the Catechol-LUMO. Figure 8 shows results for the survival probability $\rho_{MOL}(t)$, as defined in section II.C, obtained from simulations of electron injection in nanostructures extended along the [−101], [010], and [101] directions.

The electronic excitation is initialized by populating the LUMO of the catechol adsorbate anchored at the center of the extended nanostructures. Convergence with respect to the size of the system required extending the system with up to five nanostructure units.

Exponential fitting curves to $\rho_{MOL}(t)$ (see dashed lines in Figure 8) define the approximate characteristic times for the two electron-injection steps in nanostructures extended along the [−101] direction. These results indicate that the early time relaxation can be described by an ultrafast ($\tau \simeq 6$ fs) electron-injection event that involves a population decay in the molecular adsorbate to about 50−20% during the first 5−10 fs of dynamics. At longer times the electron injection is much slower and depends on the nanonstructure's extension being along the [−101], [010], and [101] crystallographic directions.

The analysis of the time-dependent charge distribution, discussed later in this section, indicates that the population of the catechol adsorbate decays during the first 5−10 fs of dynamics due to a primary electron-injection event. This process localizes the injected charge in the Ti^{4+} ions next to the adsorbate, including the hexacoordinated Ti^{4+} ion (see Figure 4) and the Ti^{4+} ions that anchor the photoexcited catechol adsorbate. The characteristic time of the primary electron-injection event is the same for all nanostructures simply because it is independent of the extension of the nanostructure along the three crystallographic directions. At longer times, however, the electron-injection rate is limited by the process of charge delocalization, i.e., the diffusion of the charge localized during the primary electron-injection event. This diffusional process is anisotropic and depends on the nanonstructure extension along the [−101], [010], and [101] crystallographic directions. It is important to note that nanostructures with distinct instantaneous configurations sampled from molecular dynamics simulations at 100 K and constant volume exhibit the same characteristic time for the primary ultrafast injection event ($\tau_1 \simeq 6$ fs) and, qualitatively, the same features observed for the slower diffusion process.

Figure 9 shows the time-dependent charge distribution projected onto the distinct atomic planes along the $\hat{x} \equiv$ [−101] and $\hat{y} \equiv$ [010] directions of the anatase semiconductor substrate, as defined by the expressions

$$\rho_{TiO_2}(x,t) = \sum_i \rho_{TiO_2}(R_i,t)\, \delta(x_i - x) \tag{7}$$

and

$$\rho_{TiO_2}(y,t) = \sum_i \rho_{TiO_2}(R_i,t)\, \delta(y_i - y) \tag{8}$$

with

$$\rho_{TiO_2}(R_i,t) = |\sum_\alpha \sum_{j,\beta} B_{i,\alpha}(t)\, B_{j,\beta}(t) S^{i,j}_{\alpha,\beta}| \tag{9}$$

where coordinate R_i indicates the position of atom i (i.e., a Ti^{4+} or O^{2-} ion). The sum over index j, in eq 9, includes all of the atoms in the extended structure except for those belonging to the initially excited catechol adsorbate. The index β accounts for all of the atomic orbitals associated with atom j. The excited catechol adsorbate is located at $x = 0$ and $y = 0$.

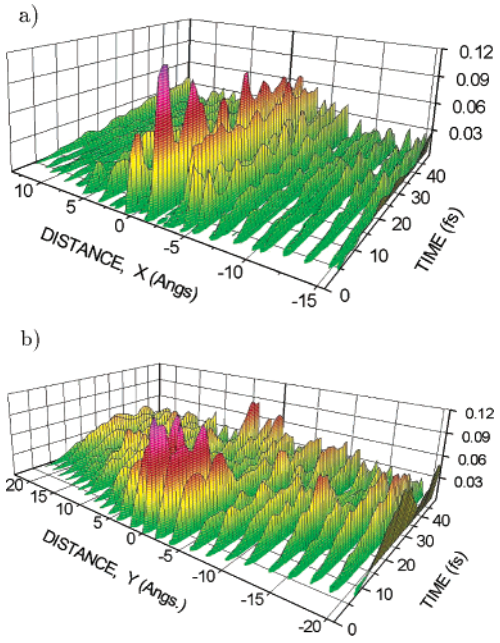

Figure 9. Time-dependent projection of the injected charge onto the $\hat{x} \equiv [-101]$ and $\hat{y} \equiv [-010]$ directions (upper and lower panel, respectively) for the first 50 fs of dynamics. The excited catechol adsorbate is located at $x = 0$ and $y = 0$.

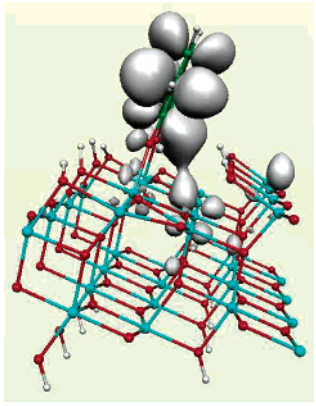

Figure 10. Instantaneous charge distribution at 2.5 fs after photoexcitation of the system to the catechol-LUMO. The electronic charge is partially injected through direct coupling to the d_{xz} orbital in the hexacoordinated Ti^{4+} ion next to the adsorbate.

The upper panel of Figure 9 ($\rho_{TiO_2}(x,t)$) shows that the charge is injected within 6 fs into the anatase ions that are next to the excited adsorbate molecule. The injected charge remains localized within about 5 Å from the adsorbate for relatively long times (i.e, $t \gtrsim 20$ fs). In contrast, the lower panel of Figure 9 shows that the injected charge is only initially localized along the [010] direction and quickly diffuses away to large distances (i.e., more than 20 Å away from the excited adsorbate molecule). The initial charge localization, along both the [−101] and [010] directions, indicates that the Ti^{4+} ions directly anchoring the excited adsorbate as well as the hexacoordinated Ti^{4+} ion next to the adsorbate (see Figures 4 and 10) play an important role in the primary electron-injection event. Figure 10 shows a snapshot of the instantaneous charge distribution at 2.5 fs after photoexcitation of the system to the catechol-LUMO. Note that there is significant hybridization between the catechol-LUMO and the d_{xz} orbital of the hexacoordinated Ti^{4+} ion next to the adsorbate. The two Ti^{4+} directly anchoring the catechol

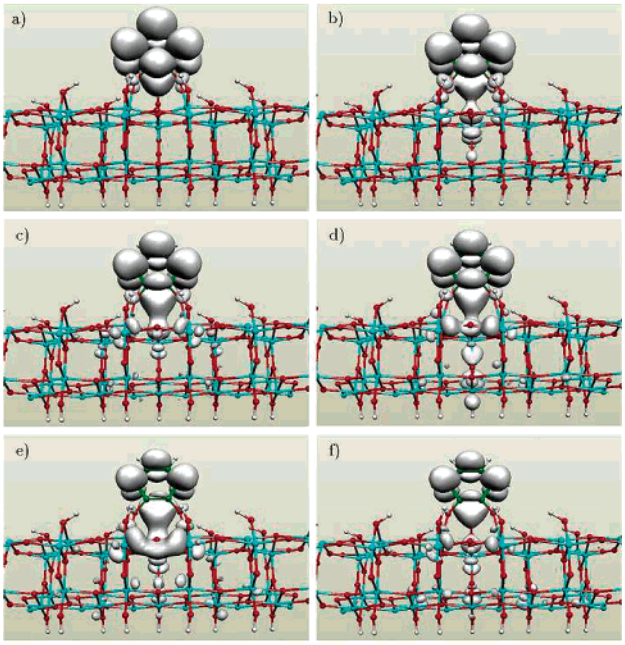

Figure 11. Evolution of time-dependent charge distribution during the early time relaxation dynamics after instantaneously populating the catechol-LUMO. The individual frames show snapshots of an electronic density isosurface at intervals of 2.5 fs.

adsorbate are also partially populated. A quantitative analysis indicates that this cluster of Ti^{4+} ions localizes 15% of the charge injected at $t = 2.5$ fs, with 10% of the charge localized in the hexacoordinated Ti^{4+} ion. A similar observation has been made by Stier and Prezhdo[26] in their study of electron injection in the isonicotinic acid/rutile interface. It is important to note, however, that both the electron-injection mechanism and the time scales for electron injection are completely different when the initial excitation is localized in the catechol-(LUMO+1). The analysis of electron injection from this electronic state is presented in section III.A.2.

Figure 11 shows the evolution of the time-dependent charge distribution during the early time relaxation dynamics after instantaneously populating the catechol-LUMO, including the primary electron-transfer event within the first 5 fs of dynamics. Note that the first three frames in Figure 11 describe the electron injection at 0, 2.5, and 5.0 fs. In addition, Figure 11 shows the nature of the subsequent relaxation mechanism, which involves surface charge separtion (i.e., diffusion along the $\hat{z} = [101]$ direction) before the injected charge diffuses along the $\hat{y} = [010]$ direction.

2. Electron Injection from the Catechol-(LUMO+1). Figure 12 shows the time-evolution of the charge distribution during the early time relaxation dynamics after instantaneously populating the orbital (LUMO+1) in the adsorbate catechol molecule.

Figure 12 shows that the electron-injection mechanism from the (LUMO+1) of catechol is completely different from the mechanism discussed in section III.A.1. Figure 12 shows that very little charge is injected in the hexacoordinated Ti^{4+} ion, in contrast to the injection mechanism from the catechol-LUMO. The electron injection proceeds through the two Ti^{4+} ions directly anchoring the adsorbate (see first three panels in Figure 12). Furthermore, the injected charge quickly delocalizes along the $\hat{y} = [010]$ direction, on the surface of the TiO_2-anatase,

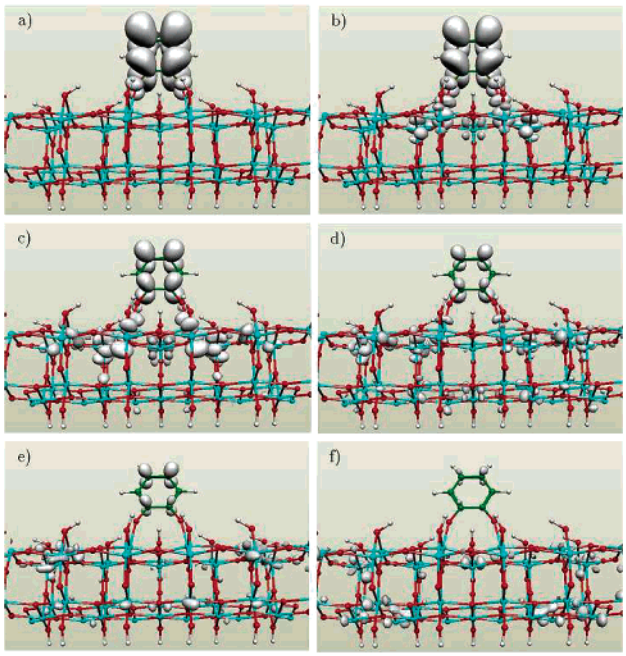

Figure 12. Evolution of time-dependent charge distribution during the early time relaxation dynamics after instantaneously populating the (LUMO+1) of a catechol adsorbate molecule. The individual frames show snapshots of an electronic density iso-surface at intervals of 2.5 fs.

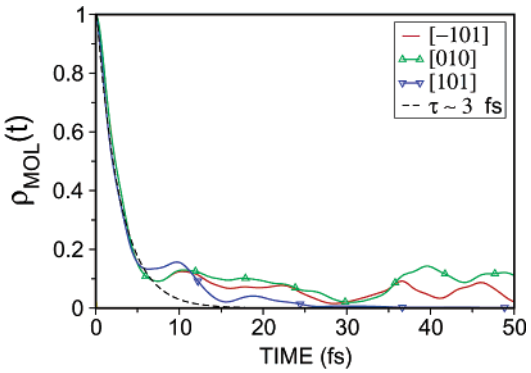

Figure 13. Time-dependent survival probability in sensitized nanostructures extended along the [−101], [010], and [101] crystallographic direction in the TiO_2 anatase crystal. The electronic excitation is initialized by populating the catechol-(LUMO+1).

before separating from the surface by delocalization along the $\hat{z} = [101]$ direction (see panels d−f in Figure 12). Note that in this case the surface relaxation mechanism gives rise to a much faster electron-injection process (i.e., the electron is completely injected within 10 fs). This relaxation mechanism is, however, less efficient than the mechanism discussed in section III.A.1 at optimizing the process of surface charge separation.

The origin of the differences observed between the two injection mechanisms can be traced back to the symmetry of the initially populated electronic state in the molecular adsorbate. The (LUMO+1) of catechol significantly couples to the d_{xz} orbitals of the two Ti^{4+} ions directly anchoring the catechol adsorbate. However, it has a nodal *xz* plane at $y = 0$ and therefore a negligible overlap with the $3d_{xz}$ atomic orbital of the hexacoordinated Ti^{4+} ion.

Figure 13 shows a quantitative description of the survival probability as a function of time after instantaneously populating the catechol-(LUMO+1) in nanostructures extended along the [−101], [010], and [101] directions in the TiO_2-anatase crystal. The time for electron injection is approximately 10 fs even in nanostructures extended along the $\hat{x} = [-101]$ direction, i.e., much faster than electron injection after instantaneously populating the catechol-(LUMO). Figure 13 shows that a single characteristic time $\tau \simeq 3$ fs describes the entire electron-transfer process when the population is initialized in the catechol-(LUMO+1) due to ultrafast relaxation of the injected charge along the $\hat{y} = [010]$ direction in the anatase surface.

B. Discussion. It has been observed in this work that an accurate description of charge delocalization requires simulations to be carried out in sufficiently extended model systems, since simulations in smaller clusters (e.g., 1.2 nm nanostructures without periodic boundary conditions) are affected by surface states that speed up the electron-injection process while the implementation of periodic boundary conditions may introduce artificial recurrencies (i.e., artifical back-electron-transfer events). Notice that a proper combination of extended structures and periodic boundary conditions have been used for all calculations throughout this work in order to obtain converged results. The computational implementation thus required the preparation of extended nanostructures with more than 600 atoms and the description of the electronic structure according to a model Hamiltonian gained from the semiempirical EH approach.

The anisotropic delocalization of the injected charge predicted by our simulations has yet to be observed experimentally. However, measurements of the electron mobility in large single crystals of TiO_2-anatase have already provided experimental evidence of anisotropy between the [100] and [001] crystallographic directions.[47] In addition, calculations of the optical properties of TiO_2-anatase near the bottom of the conduction band have revealed anisotropy between parallel and perpendicular components to the *c* axis.[48] It is, therefore, expected that new experiments in the realm of sub picosecond mid-IR/visible transient absorption spectroscopy,[50,49] or time-resolved terahertz spectroscopy,[51] might be able to probe the transient photoconductivity features evidenced by our calculations. We expect that even measurements on nanoparticles in *solutions* will show evidence of the time scales and reaction mechanisms found in our simulations, since the electronic states in the catechol/anatase complex are expected to be only slightly perturbed by the interactions with the solvent molecules.

Finally, we have shown that the electron-injection mechanisms from both the catechol-LUMO and the catechol-(LUMO+1) involve ultrafast interfacial processes where the initial population in the excited electronic state of the molecular adsorbate decays to about 50−20% in about 5−10 fs. This characteristic time for the excited-state interfacial electron transfer in catechol/anatase complexes awaits experimental verification. However, similar ultrafast electron injection times have already been measured in TiO_2 sensitized by small organic

(47) Forro, L.; Chauvet, O.; Emin, D.; Zuppiroli, L.; Berger, H.; Lévy, F. *J. Appl. Phys.* **1994**, *75*, 633.
(48) Mo, S. D.; Ching, W. Y. *Phys. Rev. B* **1995**, *51*, 13023. Asahi; et al. *Phys. Rev. B* **2000**, *61*, 7459. Beltrán; et al. *Surf. Sci.* **2001**, *490*, 116.
(49) Asbury, J. B.; Hao, E.; Wang, Y.; Gosh, H. N.; Lian, T. *J. Phys. Chem. B* **2001**, *105*, 4545.
(50) Hao, E.; Anderson, N. A.; Asbury, J. B.; Lian, T. *J. Phys. Chem. B* **2002**, *106*, 10191.
(51) Beard, M. C.; Turner, G. M.; Schmuttenmaer, C. A. *J. Phys. Chem. B* **2002**, *106*, 7146.
(52) Pan, J.; Benko, G.; Xu, Y.-H.; Pascher, T.; Sun, L. C.; Sundstrom, V.; Polivka, T. *J. Am. Chem. Soc.* **2002**, *124*, 13949.
(53) Hoertz, P. G.; Thompson, D. W.; Friedman, L. A.; Meyer, G. J. *J. Am. Chem. Soc.* **2002**, *124*, 9690.

molecules. Schnadt et al.[15] have recently obtained experimental evidence that electrons are transferred from the bi-isonicotinic acid excited states (e.g., the LUMO+1 and LUMO+2) to TiO_2-rutile within 3 fs. In addition, Huber et al.[16] have reported an interfacial electron-transfer time $\tau \simeq 6$ fs in the alizarin/TiO_2 system. These authors also emphasized that the observed electron-transfer mechanisms are mediated by the *excited* electronic states of the dye, rather than the electron being injected into the semiconductor material directly from the ground electronic state of the adsorbate.

IV. Conclusions

We have shown how to combine ab initio DFT molecular dynamics simulations with quantum dynamics calculations of electronic relaxation to investigate excited state interfacial electron-transfer dynamics in sensitized semiconductors. The approach exploits the implicit simplicity of the early time interfacial electron-transfer dynamics where nuclear motion is much slower than carrier relaxation.

Our simulation results have shown that the reaction mechanisms as well as the characteristic times for electron injection in catechol/TiO_2-anatase nanostructures are very sensitive to the symmetry of the electronic state initially populated in the adsorbate molecule, since the interfacial reaction dynamics is driven by the electronic couplings between the initially populated electronic state in the molecular adsorbate and the electronic states of similar energy in the conduction band of the semiconductor.

We found that electron injection from the catechol-LUMO involves a primary electron-transfer event that localizes the injected charge in the Ti^{4+} surface ions next to the photoexcited adsorbate molecule within the first 5 fs of dynamics. The injection dynamics, after photoexcitation to the catechol-LUMO, was found to be driven by the electronic couplings between the catechol-LUMO and the d_{xz} orbital of the nearest hexacoordinated Ti^{4+} ion. This process was followed by charge delocalization (i.e., carrier relaxation) through the anatase crystal, an anisotropic process that involved surface charge separation along the [101] direction before delocalizing the charge distribution along the [010] direction of the anatase crystal. We found that carrier relaxation along the [−101] direction can be much slower than relaxation along the [101] and [010] directions.

We have shown that, in contrast to electron injection from the catechol-LUMO, electron injection from the catechol-(LUMO+1) involves couplings with the d_{xz} orbitals of the pentacoordinated Ti^{4+} ions directly anchoring the catechol adsorbate. We found that both the initial injection and the subsequent delocalization processes are faster than the electron injection from the catechol-LUMO. Furthermore, we found that carrier relaxation after photoexcitation to the catechol-(LUMO+1) is significantly different from the charge delocalization process observed after electron injection from the catechol-LUMO. Here, carrier relaxation involves charge diffusion along the semiconductor surface (i.e., along the [010] direction in the anatase crystal) before the injected charge separates from the surface by diffusing along the [101] direction.

Acknowledgment. V.S.B. acknowledges a generous allocation of supercomputer time from the National Energy Research Scientific Computing Center and financial support from a Research Innovation Award from the Research Corporation, a Petroleum Research Fund Award (type G) from the American Chemical Society, a junior faculty award from the F. Warren Hellman Family, and start-up package funds from the Provost's office at Yale University.

JA0346330